INORGANIC CHEMISTRY
FRONTIERS

RESEARCH ARTICLE

View Article Online
View Journal

Cite this: DOI: 10.1039/d5qi00546a

Non-mutagenic Ru(II)–phosphine-based complexes induce mitochondria-mediated apoptosis in breast cancer cells: from 2D to 3D investigations†

Marcos V. Palmeira-Mello, *[a] Tamara Teixeira,[a] Analu R. Costa, [a,b] Aline Maria Machado,[c] Rone A. De Grandis,[d] Leticia P. de Oliveira,[a] Carlos A. F. Moraes,[a] João H. de Araujo-Neto, [e] Victor M. Deflon,[f] Adriano D. Andricopulo,[b] Javier Ellena,[g] Heloisa S. Selistre-de-Araújo,[c] Fillipe V. Rocha[a] and Alzir A. Batista *[a]

Received 23rd February 2025,
Accepted 6th April 2025

DOI: 10.1039/d5qi00546a

rsc.li/frontiers-inorganic

Three ruthenium(II)–phosphine-based complexes with the general formula [Ru(N–S)(dppm)$_2$]PF$_6$ (**Ru1–Ru3**) were prepared and studied as anticancer agents [N–S represents 2-mercapto-2-thiazoline (Hmtz), mercapto-1-methylimidazole (Hmmi) and 4,6-diamino-2-mercapto-pyrimidine (Hdmp), and dppm represents 1,1′-bis(diphenylphosphino)methane]. The distribution coefficients of these compounds were assessed, and log *P* values indicated their preference for the organic phase. After confirming their stability in solution, their *in vitro* cytotoxicity was investigated on different breast cell lines. Our findings revealed that **Ru2** was 50-fold more cytotoxic and almost 2-fold more selective than the cisplatin control, considering MCF-7 cells. Also, **Ru2** induced morphological changes and inhibited colony formation in this cell line. Considering the advantages of 3D cell culture models for screening new anticancer drug candidates, the effect of **Ru2**, which was found to be the best candidate compound, was investigated on multicellular tumor spheroids. A live/dead assay revealed a dead cell population in both 2D and 3D MCF-7 cell models upon treatment at the IC$_{50}$ concentration. The ruthenium–phosphine complex was able to affect cell cycle distribution and mitochondrial membrane potential, inducing apoptotic cell death. Ames and micronucleus tests indicated the absence of mutagenicity for **Ru2**. To the best of our knowledge, this work demonstrated for the first time the effects of a ruthenium–phosphine complex on MCF-7 breast cancer cells using 2D and 3D cell-based models, highlighting its potential as a promising anticancer agent.

Introduction

The use of metallodrugs as chemotherapeutic agents emerged, initially, with the development of cisplatin and was reinforced by other Pt-based complexes.[1,2] Nonetheless, despite the effectiveness of platinum compounds for chemotherapy, there is a significant effort in the search for and development of new metallodrugs based on other metals.[3–6] In this scenario, ruthenium compounds have emerged as promising alternatives for the development of new chemotherapeutic agents.[7–17] In particular, Ru–phosphine-based compounds, which are primarily studied for catalytic purposes, are being extensively investigated due to their high cytotoxicity.[18–21] The phosphine moiety is essential for enhancing the lipophilicity of these complexes, allowing their entry into the cancer cells. Furthermore, these compounds are reported to induce mitochondrial damage, which leads to apoptosis-mediated cell death.[22,23] Since the cytotoxicity of metal-based compounds depends on the nature

[a]Departament of Chemistry, Universidade Federal de São Carlos (UFSCar), São Carlos, 13565-905 SP, Brazil. E-mail: marcos.palmeira@ufscar.br, daab@ufscar.br
[b]Laboratory of Medicinal and Computational Chemistry (LQMC), Institute of Physics, Universidade de São Paulo (USP), São Carlos, 13563-120 SP, Brazil
[c]Department of Physiological Sciences, Universidade Federal de São Carlos (UFSCar), São Carlos, 13565-905 SP, Brazil
[d]School of Pharmaceutical Sciences of São Paulo State University (UNESP), Araraquara, 14800-903 SP, Brazil
[e]Department of Fundamental Chemistry, Institute of Chemistry, University of São Paulo, 05508-000 São Paulo, SP, Brazil
[f]São Carlos Institute of Chemistry, Universidade de São Paulo (USP), São Carlos, 13566-590 SP, Brazil
[g]São Carlos Institute of Physics, Universidade de São Paulo (USP), São Carlos, 13566-590 SP, Brazil

† Electronic supplementary information (ESI) available. CCDC 2235452–2235454. For ESI and crystallographic data in CIF or other electronic format see DOI: https://doi.org/10.1039/d5qi00546a

of both the metal and the ligand, coordinating bioactive molecules to a ruthenium(II) metal center is a useful strategy to develop new metal-based compounds with potential anticancer activity.[24–30] In this work, we report the synthesis of three Ru(II)–phosphine-based compounds containing different mercapto ligands. Originally obtained as chloride salts,[31] these compounds were synthesized and characterized as hexafluorophosphate salts, namely [Ru(mtz)(dppm)$_2$]PF$_6$ (**Ru1**), [Ru(mmi)(dppm)$_2$]PF$_6$ (**Ru2**) and [Ru(dmp)(dppm)$_2$]PF$_6$ (**Ru3**) (dppm = 1,1-bis(diphenylphosphine)methane, mtz = 1,3-thiazolidine-2-thione, mmi = mercapto-1-methylimidazole, and dmp = 4,6-diamino-2-mercaptopyrimidine in their deprotonated forms) (Fig. 1).

The *in vitro* cytotoxicity of **Ru1–Ru3** was investigated on breast cancer cells. Encouraged by the cytotoxicity and selectivity results, cell morphology assays were performed for **Ru2** in MCF-7 cells. Also, clonogenic, migration and zymography experiments were conducted. Considering the advantages of a 3D cellular structure in comparison with a monolayer cell culture, the effect of our promising compound (**Ru2**) was investigated on multicellular tumor spheroids.

Our findings revealed that the ruthenium–phosphine complex affected the mitochondrial membrane, leading to cell death *via* apoptosis. Furthermore, Ames and micronucleus assays indicated a lack of mutagenicity for this compound, providing fresh insights into the ruthenium(II)–phosphine scaffold as an anticancer agent.

Results and discussion

Synthesis and characterization

The ruthenium complexes (**Ru1–Ru3**) were synthesized by substituting two chlorido ligands from the precursor, *cis*-[RuCl$_2$(dppm)$_2$], with different mercapto ligands in the presence of NaHCO$_3$. The complexes were isolated as pale yellow solids, and their compositions were confirmed by elemental analyses. The IR spectra (Fig. S1–S3†) of all compounds show the presence of bands in the region of 1619–1432 cm^{-1}, ascribed to the C=C and C=N bonds of both the phosphine and mercapto ligands. The bands around 1100 cm^{-1} and 520 cm^{-1}, and 1188–1246 cm^{-1} can be assigned, respectively, to the P–C and C–S vibrations. Additionally, bands at ≈840 cm^{-1} were attributed to P–F, indicating the presence of a PF_6^- counter-ion.[32]

The $^{31}P\{^1H\}$ NMR spectra of **Ru1–Ru3** present signals assigned to the four phosphorus (P) atoms present in their structures. The ^{1}H NMR spectrum of [Ru(mtz)(dppm)$_2$]PF$_6$ (**Ru1**) shows protons from the CH$_2$ group of the 1,3-thiazolidine-2-thione ligand at δ = 2.25–3.54 ppm (Fig. 2A, indicated with red arrows). HSQC and HMBC 2D maps were useful in elucidating particular couplings related to single and multiple hydrogen–carbon correlations. In this map, correlations between the CH$_2$ carbons from 1,3-thiazolidine-2-thione at δ = 59.60 ppm and 31.08 ppm and the respective attached protons at δ = 2.25 and 3.54 ppm and at δ = 2.37 and 3.21 ppm were observed. The CH$_2$ carbons from the diphosphine ligands at δ = 41.23 and 41.50 ppm were assigned based on their correlation with the protons at δ = 4.27 and 5.27 ppm and at δ = 4.44 and 5.35 ppm, respectively (Fig. 2B). A similar behavior was observed for **Ru2** and **Ru3**. For [Ru(mmi)(dppm)$_2$]PF$_6$ (**Ru2**), the protons at δ = 3.17 ppm, 5.70 ppm and 6.74 ppm were correlated with carbons at δ = 30.68 ppm, 124.74 ppm and 118.80 ppm, respectively. Finally, an HSQC correlation between the CH carbon from 4,6-diamino-2-mercapto-pyrimidine at δ = 79.04 ppm and its attached proton at δ = 4.99 ppm was observed for [Ru(dmp)(dppm)$_2$]PF$_6$ (**Ru3**) (Fig. S4–S16†). These results are in agreement with the molar conductance obtained in DMSO, which supported these compounds as hexafluorophosphate salts of the 1 : 1 electrolyte type.[33]

The UV-Vis spectra recorded in DMSO are similar to those already reported for other ruthenium(II)–phosphine complexes containing mercapto ligands.[30,31] Bands around 350 nm can be ascribed to metal-to-ligand charge transfer transitions (MLCT). In addition, bands around 400 nm were observed and attributed to MLCT and d–d mixing transitions (Fig. S17–S19†). The ESI-MS spectra of **Ru1–Ru3** (Fig. S20–S22†) show peaks for the molecular ions of [Ru(mtz)(dppm)$_2$]$^+$, [Ru(mmi)(dppm)$_2$]$^+$ and [Ru(dmp)(dppm)$_2$]$^+$ at (m/z^+) 988.1239, 983.1646 and 1011.1718, respectively.

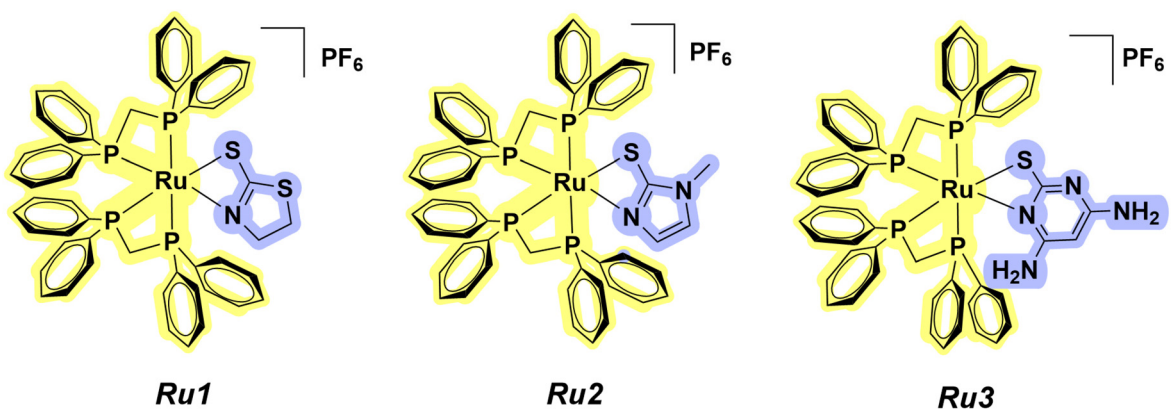

Fig. 1 Chemical structures of compounds **Ru1–Ru3**.

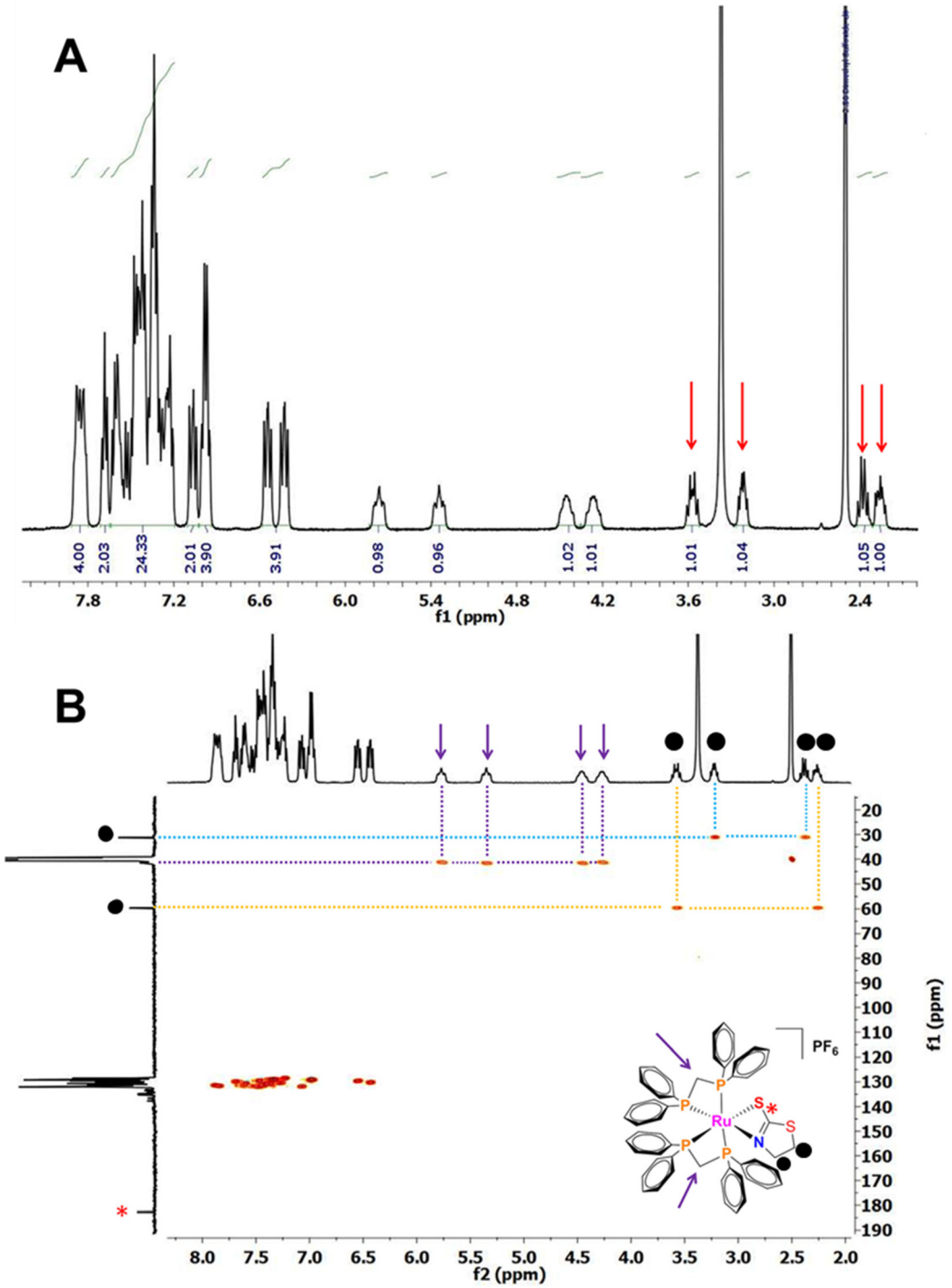

Fig. 2 (A) ^{1}H NMR spectrum and (B) $^{1}H-^{13}C$ HSQC correlation map of compound $[Ru(mtz)(dppm)_2]PF_6$ (**Ru1**) in DMSO-d_6 at 298 K.

The electrochemical behavior of **Ru1–Ru3** complexes was investigated by cyclic voltammetry (CV). Measurements in DCM at 50 mV s^{-1} revealed *quasi*-reversible processes, associated with the Ru(II)/Ru(III) couple (Fig. S23–S25†). The E_{pa} (anodic peak potential) observed for **Ru1–Ru3** lies in the range 1.08–1.38 V *vs.* Ag/AgCl, which is in accordance with values already reported for similar Ru(II)–phosphine compounds[24] (Table S1†).

Monocrystals have been obtained for **Ru1–Ru3**, and their solid structures have been solved by X-ray crystallography. The complexes crystallize in the monoclinic system for **Ru1** ($P2_1/c$) and **Ru2** ($C2/c$) and in the triclinic system for **Ru3** ($P\bar{1}$), with one molecule per asymmetric unit. As shown in Fig. 3, the obtained crystal structures of the complexes corroborate with the results from other characterization techniques, displaying the same coordination mode for the three ligands (N–S). In all

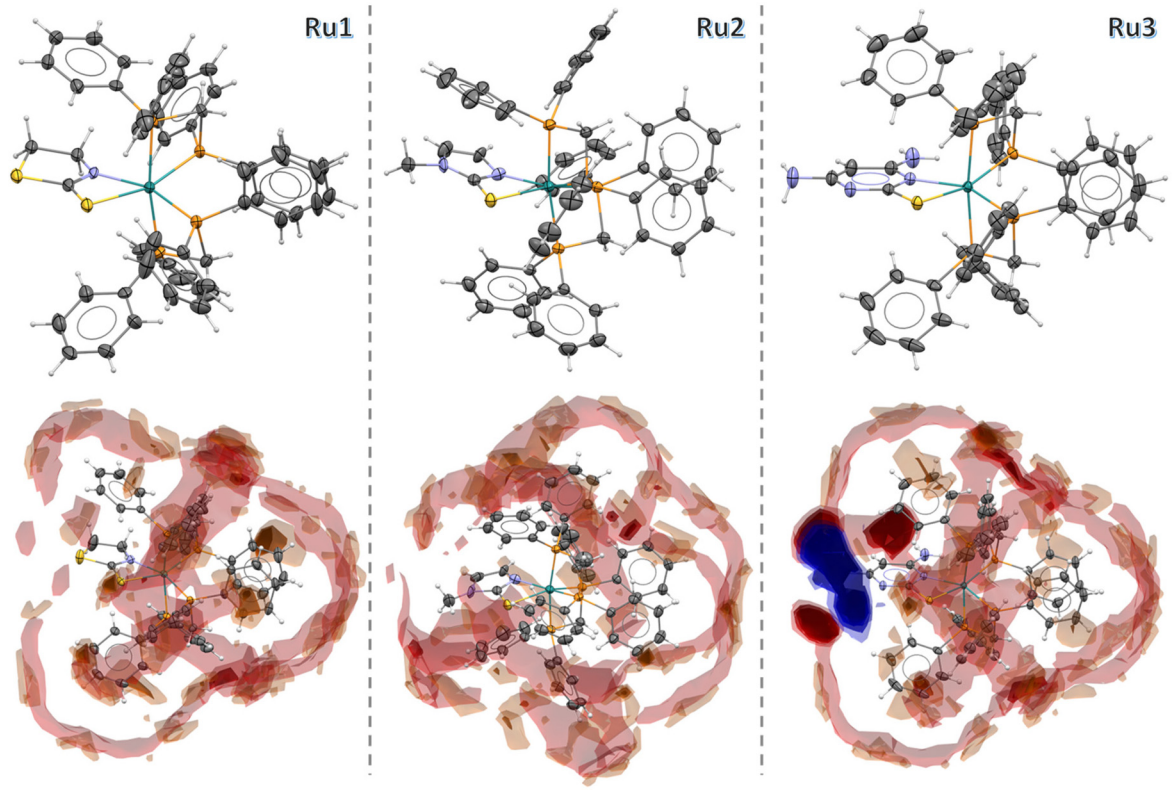

Fig. 3 Crystal structure and Full Interaction Maps of the complexes **Ru1**, **Ru2** and **Ru3**. The ellipsoids are represented at 30% of probability and the PF_6^- anions are omitted.

cases, the ruthenium metal center adopts a distorted octahedral geometry, evidenced by the bond angles around the Ru atom, displaying values far from the expected ideal angle (90°). The P1–Ru1–P2 and P3–Ru1–P4 angles range between 71 and 73°, while N1–Ru1–S1 displays bond angles close to 63°. The bond lengths for **Ru1**, **Ru2** and **Ru3** are as follows: Ru1–S1 [≈2.46 Å], Ru–N1 [≈2.18 Å] and Ru–P [≈2.31 Å]. All bond lengths are in agreement with those found for similar Ru(II) complexes reported in the literature.[26,28] It should be mentioned that the structures for compounds $[Ru(mtz)(dppm)_2]Cl$ and $[Ru(mmi)(dppm)_2]Cl$ have been previously reported, and they exhibit similar features to those reported in this work for compounds containing a hexafluorophosphate counterion.[31] For more information, see Tables S2 and S3.†

The Full Interaction Maps analysis, performed using the Mercury program,[34] offered valuable insights into the intermolecular interaction patterns of the **Ru1**, **Ru2**, and **Ru3** complexes. By examining the structures with uncharged NH nitrogen, carbonyl oxygen, and aromatic CH carbon probes, distinct interaction trends were identified. In the generated maps, red regions indicate areas with a high probability of hydrogen bond acceptors, blue regions correspond to hydrogen bond donors, and brown areas highlight hydrophobic regions. The interaction profiles vary among the complexes: **Ru1** and **Ru2** are characterized by a dominance of red and brown regions, suggesting a strong hydrophobic nature, with interactions primarily governed by dispersion forces and weak hydrogen bonding. In contrast, **Ru3** displays prominent blue regions, emphasizing the hydrophilic character of its uncoordinated aromatic nitrogen acceptor, while the intense red areas surrounding NH_2 groups indicate strong hydrogen bond donor capabilities. These observations provide a comprehensive understanding of the differing interaction behaviors among the studied complexes.

Stability in solution and partition coefficient

The stability of the compounds was assessed prior to the biological studies. First, $^{31}P\{^1H\}$ NMR experiments were conducted for **Ru1–Ru3** in DMSO and DMSO/cell culture medium solutions for 48 h. No changes were observed in their spectra, suggesting the stability of the complexes under these conditions. To gain more insights into their behavior in biological environments, solutions of the complexes were also monitored by UV-Vis in DMSO/cell culture medium solutions. As no significant changes were observed, their stability was confirmed during this period (Fig. S26–S34†). After confirming the stability of all complexes, their distribution coefficient values ($\log P_{o/w}$) were assessed in octanol/water. Lipophilicity is an important physicochemical descriptor related to the capacity of a drug to penetrate the lipid bilayer and is generally associated with better accumulation in cells. Our results revealed positive $\log P$ values (Table 1), indicating their preference for

Table 1 *In vitro* cytotoxicity (IC_{50}, μM) on MDA-MB-231, MCF-7 and MCF-10A cell lines after 48 h of incubation, SI and log *P* values of compounds **Ru1–Ru3** for different cell lines. SI^1 = IC_{50} MCF-10A/IC_{50} MDA-MB-231 and SI^2 = IC_{50} MCF-10A/IC_{50} MCF-7

Complex	MDA-MB-231	MCF-7	MCF-10A	SI^1	SI^2	Log *P*
Ru1	0.31 ± 0.13	0.21 ± 0.02	0.53 ± 0.19	1.7	2.5	1.22 ± 0.02
Ru2	0.77 ± 0.16	0.28 ± 0.03	0.75 ± 0.20	0.97	2.7	0.91 ± 0.10
Ru3	1.62 ± 0.29	1.27 ± 0.17	1.87 ± 0.52	1.1	1.5	0.98 ± 0.14
Hmtz	>100	>100	>100	—	—	—
Hmmi	>100	>100	>100	—	—	—
Hdmp	>100	>100	>100	—	—	—
cis-[$RuCl_2(dppm)_2$]	1.10 ± 0.09	1.17 ± 0.21	3.11 ± 0.04	—	—	—
Cisplatin	12.43 ± 0.20	13.98 ± 0.40	23.90 ± 0.70	0.96	1.7	—

the organic phase. Similar behavior has been reported for analogous Ru(II)–phosphine compounds.[35]

Biological investigation

Cytotoxicity and morphological assays. The anticancer activity of the ruthenium complexes **Ru1–Ru3** was assessed in two human breast cancer cell lines: MDA-MB-231 (estrogen receptor-negative, ER–) and MCF-7 (estrogen receptor-positive, ER+), as well as in the non-tumorigenic epithelial cell line MCF-10A, following 48 hours of incubation. The cytotoxicity data, expressed as IC_{50} values (±SD), are summarized in Table 1. Overall, **Ru1–Ru3** showed stronger cytotoxic effects than the precursor complex *cis*-[$RuCl_2(dppm)_2$], the clinically used cisplatin, and the corresponding free mercapto ligands reported previously.[28,30] These results are consistent with our earlier findings and reinforce the therapeutic potential of this class of compounds.[31] Among the tested cell lines, MCF-7 cells were particularly sensitive to **Ru1–Ru3**, with IC_{50} values ranging from 0.28 to 1.27 μM. This represents an improvement of at least 17-, 18-, and 6-fold, respectively, over their dppe-based analogues, underscoring the importance of the diphosphine ligand in modulating biological activity (dppe = 1,2-bis(diphenylphosphino)ethane).[24] When compared to other mono-diphosphine ruthenium complexes, such as [$Ru(mtz)_2(dppb)$]PF_6, [$Ru(mmi)_2(dppb)$]PF_6, and [$Ru(dmp)_2(dppb)$]PF_6, which have IC_{50} values between 12 and 200 μM, the potency of **Ru1–Ru3** is notably higher (dppb = 1,4-bis(diphenylphosphino)butane).[36] These findings suggest that the incorporation of two chelating dppm ligands contributes to improved activity, possibly by enhancing lipophilicity, uptake, or interactions with intracellular targets.

A clear difference in activity was observed between the two cancer cell lines, with MCF-7 cells (ER+) consistently more sensitive than MDA-MB-231 cells (ER–). This is in line with known variations in drug response among breast cancer subtypes.[6,37] Within the series, **Ru1**—containing the 1,3-thiazolidine-2-thione (mtz) ligand—was the most active, followed by **Ru2** (mmi) and **Ru3** (dmp), suggesting that subtle differences in the sulfur-donor heterocycle may influence biological performance. To evaluate selectivity, **Ru1–Ru3** were also tested against MCF-10A cells. **Ru2** stood out as the most selective, with a selectivity index (SI) of 2.7 for MCF-7 cells—higher than that observed for cisplatin (SI = 1.7). Notably, **Ru2** was 18 times more selective than its dppe-containing analogue [Ru(mmi)(dppe)$_2$]PF_6,[36] further emphasizing the role of ligand design in tuning selectivity. Based on its promising cytotoxicity and selectivity profile, **Ru2** was selected for further biological investigations, including mechanistic studies.

The morphology of MCF-7 breast cells was studied in the absence and presence of **Ru2** after 48 h of treatment. As presented in Fig. 4A, significant alterations in the shape of the cells are observed at the IC_{50} concentration, and non-adherent and spherical cells are observed primarily at 2 × IC_{50} concentration after 48 h of treatment, indicating cell damage.[38] Next, cells were treated with 4′,6′-diamino-2-phenylindole (DAPI) and Green Plasma. DAPI is a dye used for nuclear staining due its capacity to bind adenine–thymine regions, while Green Plasma is commonly used for plasma membrane staining. As shown in Fig. 4B, the MCF-7 cell density reduction is accompanied by the shortening of the membrane in a concentration-dependent manner.

Our data show that treatment with the Ru(II) phosphine complex did not lead to noticeable alterations in nuclear morphology, as observed by nuclear staining assays. This finding suggests that the nucleus is not the main target of these compounds, aligning with previous studies indicating that Ru(II) phosphine complexes do not primarily act through DNA damage or chromatin disruption.[31,39]

The maintained nuclear structure after treatment supports the idea that these complexes might act through extranuclear mechanisms, possibly involving oxidative stress, mitochondrial damage, or other pathways that affect cell survival. To complement these observations, we carried out a live/dead assay using calcein AM and propidium iodide (PI) under the same conditions. As shown in Fig. 4C, treatment with **Ru2** at its IC_{50} concentration produced a mix of live (calcein-positive) and dead (PI-positive) cells, indicating partial but clear cytotoxicity. When the concentration was doubled (2 × IC_{50}), the number of PI-positive cells increased significantly, suggesting greater loss of membrane integrity and enhanced cell death.

These results point to a dose-dependent cytotoxic effect of **Ru2**, likely involving disruption of plasma membrane integrity rather than classical apoptotic pathways. Since we did not observe nuclear fragmentation, it seems likely that **Ru2** may trigger alternative, non-caspase-dependent forms of cell death. This mechanism distinguishes it from drugs like cisplatin and is in line with reports on other metal-based agents with non-conventional modes of action.

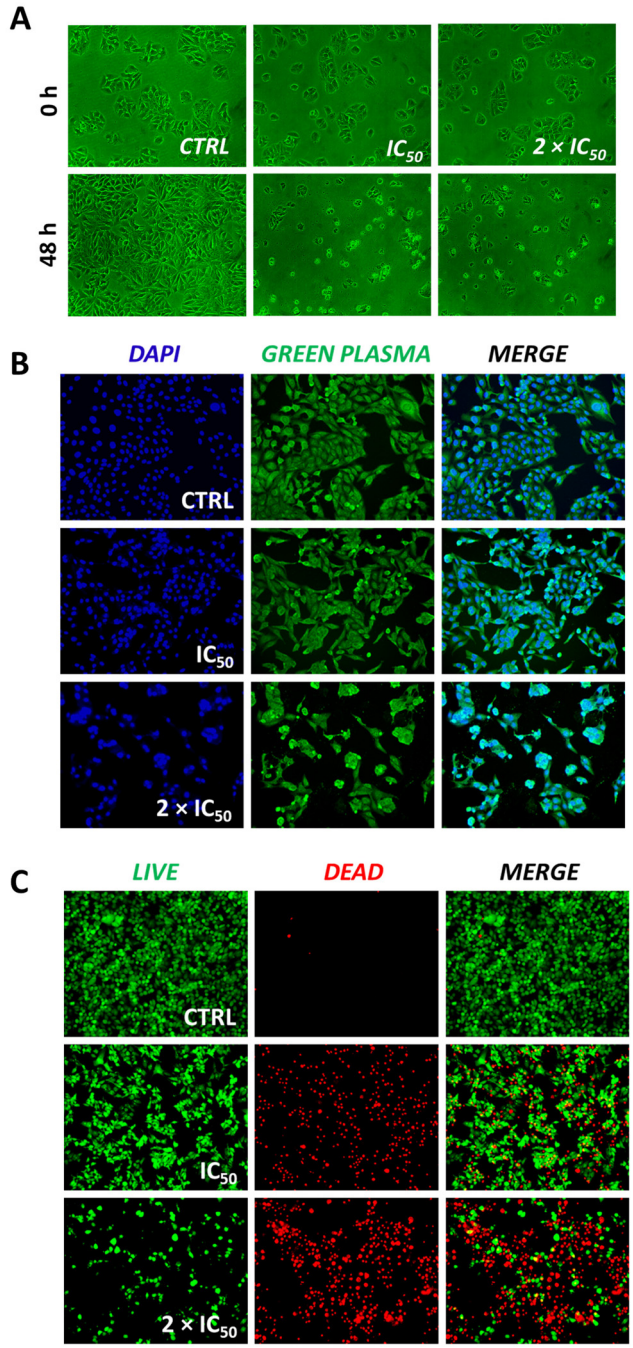

Fig. 4 (A) Microscopy images showing the cellular morphology of MCF-7 cells after 0 and 48 h in the absence (CTRL) and presence of **Ru2** at IC_{50} and 2 × IC_{50} concentrations (0.28 μM and 0.56 μM, respectively). (B) Fluorescence microscopy images of MCF-7 cells upon incubation with DAPI and Green Plasma in the absence (CTRL) and presence of **Ru2** at IC_{50} and 2 × IC_{50} concentrations. (C) Fluorescence microscopy images of MCF-7 cells upon incubation with calcein AM and propidium iodide (PI) in the absence (CTRL) and presence of **Ru2** at IC_{50} and 2 × IC_{50} concentrations. The negative controls were treated with the DMSO vehicle (0.5% v/v).

3D multicellular tumor spheroids (MCTSs)

Given the promising cytotoxic effect of **Ru2** in 2D monolayer cultures of breast cancer cells, we next examined its activity in a more physiologically relevant 3D model using multicellular tumor spheroids (MCTSs). This model better mimics the *in vivo* tumor conditions by incorporating features like 3D cell architecture, gradients in proliferation, oxygen, and nutrients. Because of these characteristics, MCTSs offer a more realistic platform for evaluating anticancer activity compared to conventional monolayer systems.[13,39]

MCF-7 spheroids were generated using a magnetic levitation system, which facilitated the aggregation of magnetized cells into uniform spheroids. At the start of the experiment, spheroids had an average diameter of 484 ± 20 μm and were treated with **Ru2** at concentrations of 0.14, 0.28, 0.56, and 1.12 μM for six days. In untreated controls, spheroids continued to grow, reaching 556 ± 26 μm in diameter.

In contrast, treatment with **Ru2** at or above its 2D IC_{50} (0.28 μM) reduced spheroid growth. The most pronounced effect was observed at 1.12 μM, where the average diameter dropped to 468 ± 13 μm (Fig. 5A and B). Concentrations below the IC_{50} had little impact on growth, suggesting that higher doses are needed to reach sufficient diffusion and activity in the 3D context. To evaluate cell viability within the spheroid structure, we performed calcein AM/propidium iodide (PI) staining. In control spheroids, most cells were viable (green fluorescence). However, **Ru2** treatment led to a noticeable increase in dead (PI-positive) cells, especially at higher concentrations (Fig. 6). These results indicate that **Ru2** can penetrate into the inner regions of the spheroid and exert cytotoxic effects, including in the less accessible, hypoxic core.

Altogether, the cytotoxic effect of **Ru2** seen in 2D cultures was confirmed in the 3D model, suggesting its potential to act in more complex tumor-like environments. Although we did not determine an IC_{50} value in the spheroid system, the inhibitory effect on growth and increased cell death provide a strong indication of its *in vivo* relevance. These findings support the further evaluation of **Ru2** in animal models and reinforce its potential as a preclinical anticancer candidate.

Clonogenic, transwell migration and zymography assays

In the next step, the anti-proliferative potential of **Ru2** was investigated. For this, the colony formation assay was explored.[40] MCF-7 cells were treated with **Ru2** at different concentrations. The ruthenium compound was removed after 2 days, the culture medium was replaced with fresh medium, and the colonies formed after 10 days were stained with violet blue, washed and dried. The results revealed a decrease in cell survival upon treatment with **Ru2** at 0.28 μM (Fig. 7A). Also, the number and the size of the colonies were drastically reduced, mainly at the IC_{50} concentration, revealing the cytotoxic and cytostatic activities of **Ru2** (Fig. 7B and C). These results are in accordance with those obtained for similar Ru (II)–phoshine compounds on different cancer cell lines.[23,28,31,41] The metastatic cascade process involves several

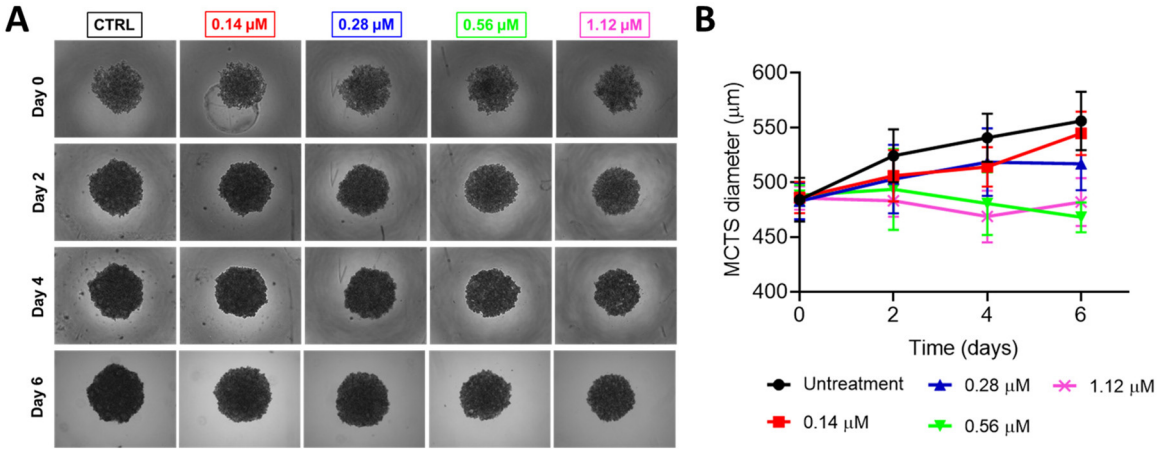

Fig. 5 (A) Changes in the growth kinetics of MCTSs treated with **Ru2** at different concentrations (0.14, 0.28, 0.56, and 1.12 μM). Images were taken after 0, 2, 4, and 6 days. (B) MCTS diameter measured at different time points (n = 8). The images were taken using a CELENA® S Digital Imaging System (Logos Biosystems) and recorded at 4× zoom.

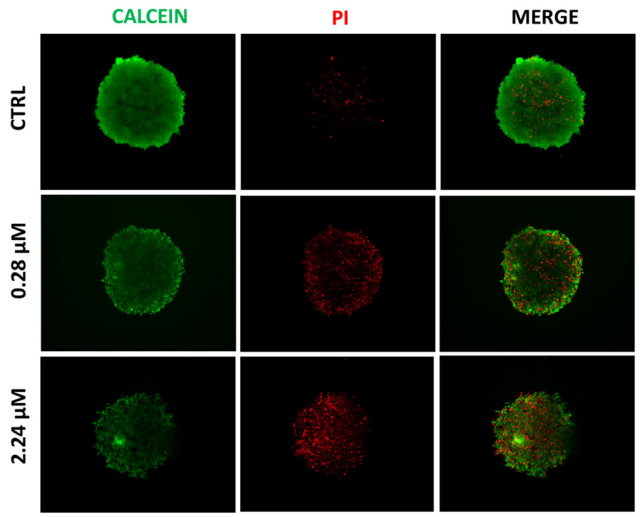

Fig. 6 Representative images of MCF-7 multicellular tumor spheroids after treatment with **Ru2** at 0.28 and 2.24 μM for 6 days and stained with a live cell marker (calcein AM, green) and a dead cell marker (propidium iodide, red). The images were taken using a CELENA® S Digital Imaging System (Logos Biosystems) and recorded at 4× zoom.

steps, such as invasion, migration, circulation and dissemination.[42] Moreover, metastasis represents more than 90% of cancer-related deaths. In this context, the anti-migratory potential of **Ru2** was also investigated *via* a transwell migration assay. MCF-7 cells were treated with **Ru2** at concentrations lower than IC_{50} to avoid cell death. The cells that migrated were stained with 4′,6′-diamino-2-phenylindole (DAPI) and counted. No significant difference was observed between the controls and the cells treated with **Ru2**, suggesting that this compound is not able to inhibit MCF-7 migration through the membrane (Fig. 7D). Subsequently, to gain more insights into the metastasis process, a gelatin zymography assay was performed. Zymography is a technique used to evaluate the secretion of matrix metalloproteinases (MMPs). Increased levels of MMPs, such as MMP-2 and MMP-9, are found in several types of cancer, and play crucial roles in cell proliferation and migration.[43] The secretory activity of these proteins was investigated after treatment with **Ru2** at concentrations lower than IC_{50}. Unfortunately, different from other ruthenium (II)-based compounds,[43,44] our results suggest that **Ru2** did not inhibit the secretion of MMP-2 in MCF-7 cells (Fig. 7E and F). It should be mentioned that MCF-7 cells have low invasive and migration capacities,[45] which may also have an impact on the secretion of metalloproteinases. In this scenario, the anti-migratory potential of **Ru2** could be studied further under different conditions.

Mechanism of action

Considering the promising results obtained for **Ru2**, several biological experiments were performed to gain insights into its mechanism of action in MCF-7 cancer cells. Firstly, the cell cycle distribution was assessed by flow cytometry in the absence and presence of the ruthenium compound. Most untreated cells were found in the G1 phase (~ 52%). Our results revealed that **Ru2** induced arrest in the G1 phase in a concentration-dependent manner, altering this cell population at the expense of both S and G2/M phases (Fig. 8A).[46] Although DNA remains the main studied target for metal-based compounds, previous experiments revealed a lack of covalent interaction between this biomolecule and ruthenium (II)–phosphine compounds.[31] Additionally, the nucleus appears unharmed upon DAPI/Green Plasma staining (see Fig. 4B), indicating that **Ru2** does not primarily target it. In this scenario, we decided to investigate the mitochondria. We studied the capacity of **Ru2** to affect the mitochondrial membrane potential (MMP, $\Delta\psi_m$) of MCF-7 cells. To evaluate its integrity, we analyzed the JC-1 signal upon accumulation in this organelle. Both aggregate and monomeric forms of JC-1 dye are found depending on the mitochondrial status. As

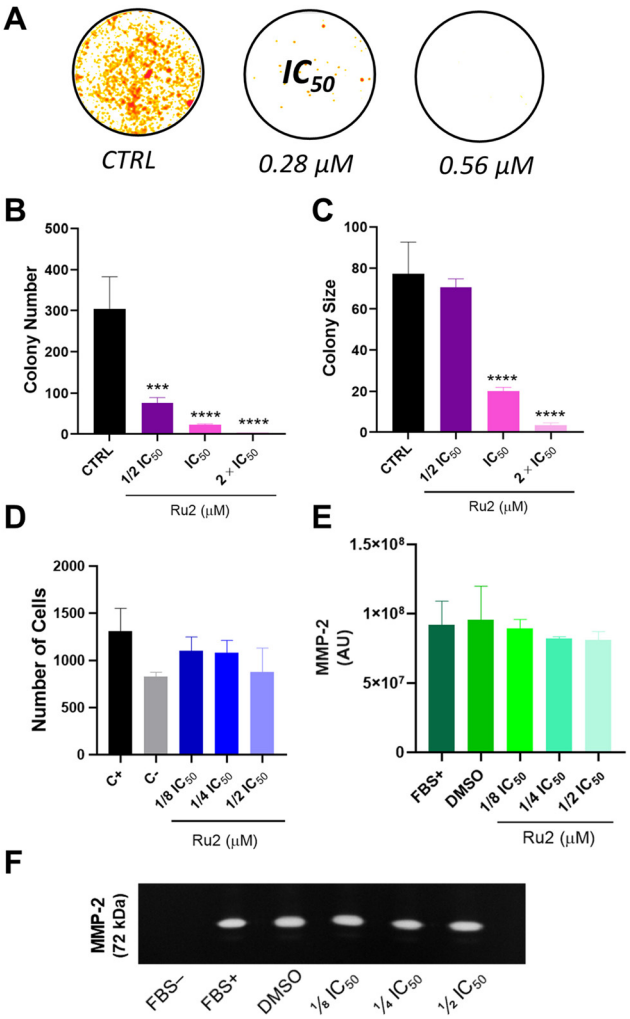

Fig. 7 (A) Representative colony formation images, and quantitative data representing the (B) colony number and (C) size of MCF-7 cells in the absence (CTRL) and presence of **Ru2** at $\frac{1}{2} \times IC_{50}$, IC_{50} and $2 \times IC_{50}$ concentrations. (D) Number of migrating cells after 24 h of incubation with **Ru2** at $\frac{1}{8} \times IC_{50}$, $\frac{1}{4} \times IC_{50}$ and $\frac{1}{2} \times IC_{50}$ concentrations. The negative control is RPMI (FBS−), and the positive control is RPMI/FBS (FBS+). The study was performed in duplicate, and the image represents one of them. (E) Bar graph and (F) gelatin zymography of MMP-2 activity relative to MCF-7 cells after 24 h of incubation with **Ru2** at $\frac{1}{8} \times IC_{50}$, $\frac{1}{4} \times IC_{50}$ and $\frac{1}{2} \times IC_{50}$ concentrations. The results are compared with the negative control (FBS−) and positive control (FBS+). DMSO vehicle (0.5% v/v) was used in all experiments. Data are expressed as mean ± SD or SEM of two or three independent measurements. The statistical analysis was performed with one-way ANOVA followed by Dunnett's test (***$p < 0.001$ and ****$p < 0.0001$).

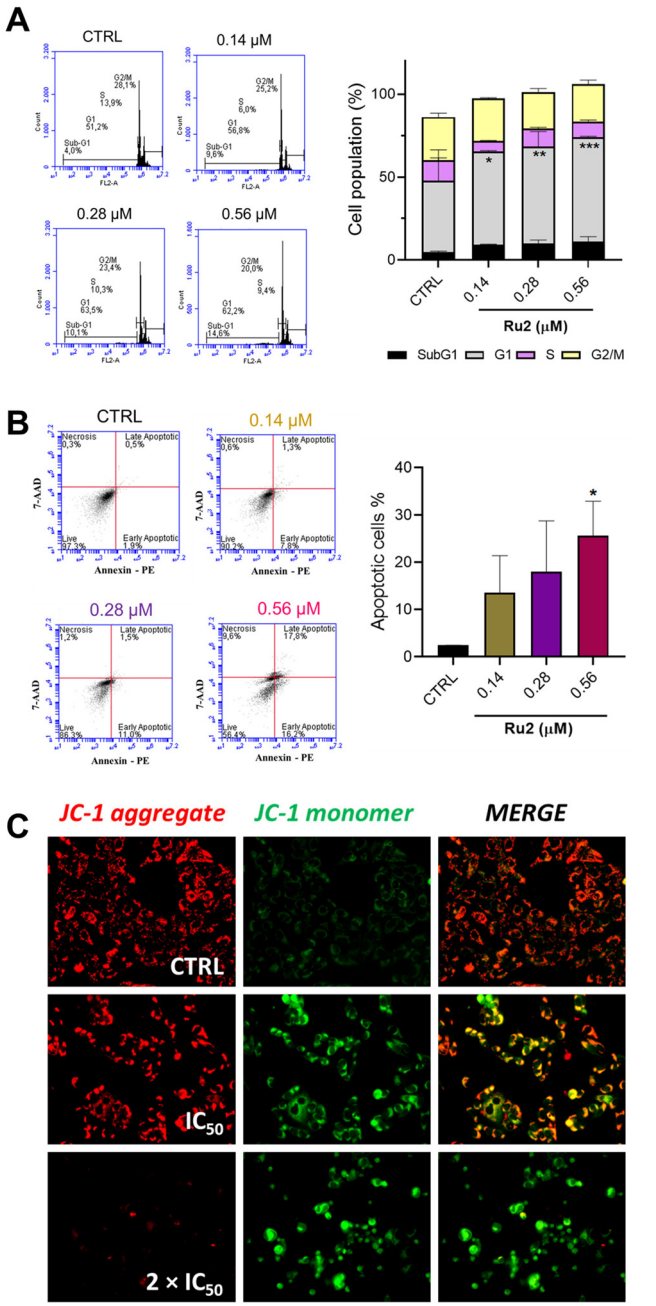

Fig. 8 Investigation of the mechanism of action of **Ru2**. (A) Cell cycle distribution on MCF-7 cells and percentage of cell population in each phase of the cycle after 48 h of treatment with **Ru2** at $\frac{1}{2} \times IC_{50}$, IC_{50} and $2 \times IC_{50}$ concentrations. The statistical analysis was performed with two-way ANOVA followed by Dunnett's test (*$p < 0.01$; **$p < 0.001$; ***$p < 0.003$). (B) Apoptosis/necrosis assay. Representative dot plot figures of the cell populations (necrosis; late apoptotic; early apoptotic and live cells), and quantification of percentage total apoptotic cells after 48 h of treatment with **Ru2** at $\frac{1}{2} \times IC_{50}$, IC_{50} and $2 \times IC_{50}$ concentrations. The statistical analysis was performed with one-way ANOVA followed by Dunnett's test (*$p < 0.02$). Data are expressed as mean ± SD of the assays in triplicate. (C) Fluorescence microscope analysis of MMP levels by JC-1 staining on MCF-7 cells after 24 h of treatment with **Ru2** at IC_{50} and $2 \times IC_{50}$ concentrations.

expected, in healthy mitochondria, the aggregate form rises and emits a red fluorescence. However, after treatment with **Ru2** for 24 h, a monomeric form is seen as a result of mitochondrial damage, identified by a green fluorescence. As reported for several Ru(II)–phosphine compounds, this MMP imbalance is an important feature of apoptotic cell death.[23,47] In this context, to assess whether **Ru2** induces apoptosis in MCF-7 cells, flow cytometry analysis was performed following

treatment with increasing concentrations of the compound (0.14–0.56 μM). Cells were stained with Annexin V-PE and 7-AAD to distinguish early and late apoptotic populations. A clear, dose-dependent increase in apoptosis was observed, with the proportion of Annexin V-positive cells reaching approximately 34% at 0.56 μM (Fig. 8B and C). These findings support the ability of **Ru2** to activate apoptotic pathways, likely *via* a mitochondrial-mediated mechanism. This is in agreement with previous studies reporting similar effects for ruthenium–phosphine complexes in other cancer cell lines.[23,31] While the current data point towards the activation of intrinsic apoptosis, we do not exclude the involvement of alternative or complementary mechanisms, given the complexity of cell death pathways and the multifaceted nature of metal-based drug action.

Genotoxicity studies

Genotoxicity experiments are crucial in drug discovery and development as substances can be harmful to the cells and damage genetic information. For this purpose, Ames and micronucleus tests were conducted. The mutagenicity of **Ru2** was assessed by the *Salmonella*/microsome assay (Ames test) using five bacterial strains (*S. typhimurium* TA1535, TA98, TA100, TA97a, and TA102). The Ames test is a widely accepted short-term bacterial assay for identifying substances that can produce genetic damage that leads to gene mutations. Moreover, it is one of the mutagenic assays recommended by regulatory agencies such as the FDA (Food and Drug Administration), which aims to ensure the safety of new drugs.[48] Each strain carries different mutations in various genes in the histidine operon, according to international guidelines.[49] A metabolic activation system (S9 mix) was added to *S. typhimurium* during the assay to metabolize the compounds by cytochrome P450.

The mean number of revertants/plate (M), the standard deviation (SD), and the mutagenic index (MI) after treatment with different concentrations of **Ru2** are presented. The treatment did not present substantial alterations in the number of revertant colonies compared to the negative control (Fig. 9A). Also, the ruthenium compound did not show an MI > 2.0, revealing the lack of mutagenicity at the tested concentrations (Fig. 9B).

Micronuclei are small DNA-containing nuclear structures resulting from chromosomal breaks or whole chromosomes that are lagging in anaphase due to mitotic errors or DNA damage.[50] The CBPI is a biological index for detecting a cell cycle delay or reduction of cell proliferation. The micronucleus assay was used to determine the mutagenic potential of **Ru2**, and the results obtained using the human hepatocellular carcinoma HepG2 cell line are shown in Table 2. The frequency of micronuclei (MNfreq) evidenced that **Ru2** did not induce chromosomal instability in HepG2 cells at assayed concentrations. The positive control (doxorubicin) caused a significant increase in MNfreq compared to the control group ($p > 0.05$). Moreover, the cytokinesis-block proliferation index (CBPI) decreased significantly in cells treated with the higher concentration of **Ru2** compared to the control. Similarly, the percen-

Table 2 Frequency of micronuclei (MNfreq), percentage of binucleate cells (BN), cytokinesis-block proliferation index (CBPI), and percentage of cytotoxicity in HepG2 cells treated with different concentrations of **Ru2**. Values are expressed as mean ± SD ($n = 3$) based on three independent experiments. C−; negative control, PBS in culture medium; C+: positive control, doxorubicin at 0.05 μM. * Significantly different from the C− ($p < 0.05$; Kruskal–Wallis test)

Treatment	MNfreq	%BN	CBPI	% Cytotoxicity
C−	11.07 ± 3.00	58.70 ± 6.85	1.82 ± 0.02	
C+	44.12 ± 5.02*	45.33 ± 4.33*	1.61 ± 0.07*	19.00 ± 2.01
0.12 μM	8.33 ± 0.14	57.95 ± 5.44	1.81 ± 0.04	2.30 ± 0.14
0.25 μM	12.40 ± 1.88	53.10 ± 2.76	1.79 ± 0.02	5.01 ± 1.13
0.50 μM	9.33 ± 1.33	43.33 ± 1.13*	1.58 ± 0.18*	26.75 ± 3.59

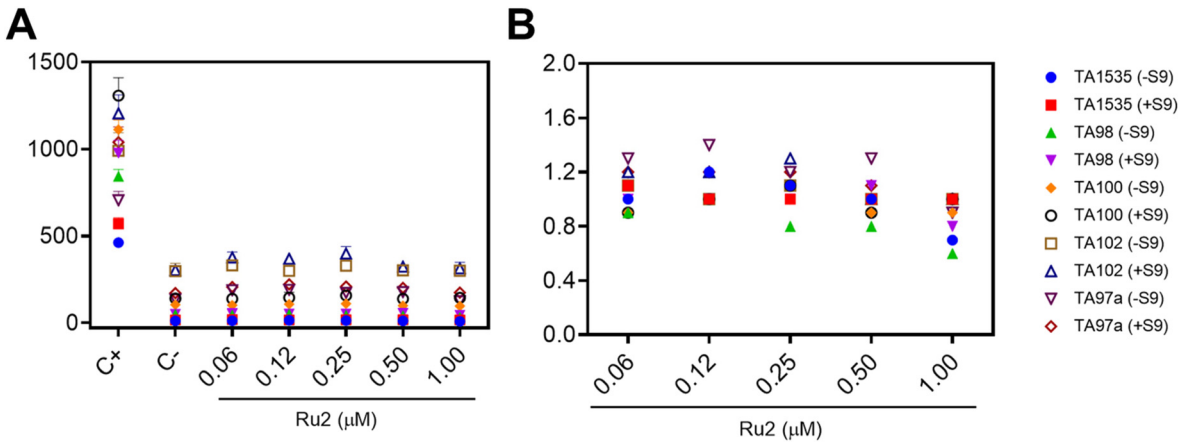

Fig. 9 Mutagenic activity expressed as the number of revertants per plate (A) and mutagenic index (B) in *Salmonella typhimurium* strains TA1535, TA98, TA100, TA102, and TA97a treated with **Ru2** at different concentrations in the absence (−S9) or presence (+S9) of metabolic activation. Negative control (C−): DMSO (100 μL per plate); positive control (C+): 4-nitro-*O*-phenylenediamine (24 μM, TA98 and TA97a), sodium azide (7 μM, TA1535 and TA100), and mitomycin (0.53 μM, TA102) for −S9, and 2-anthramine (2.3 μM, TA1535, TA98, TA100, and TA97a) and 2-aminofluorene (20 μM, TA102) for +S9. The assay was performed in triplicate.

tage of binucleate cells (%BN) was significantly lower in the cells treated with 0.5 μM of **Ru2** in comparison with the negative control, while at the same concentration, the percentage of cytotoxicity reached 26.75%.

Our results indicated that, even without detecting mutagenic effects in the MN assay, a cytostatic effect of **Ru2** at 0.5 μM was detected in HepG2 cells after 24 h of treatment, as measured by the cytokinesis-block proliferation index (CBPI). The frequency of micronuclei and the cytokinesis-block proliferation index have consistently been used as biomarkers of chromosomal damage. This effect after adding **Ru2** could be due to increased apoptotic or necrotic events in HepG2 cells.[51] Overall, our results indicate that **Ru2** exhibits no mutagenic effects, as observed for other Ru(II)-based complexes.[27,52]

Conclusions

In summary, we have prepared three ruthenium(II)–diphosphine complexes and investigated them as potential anticancer candidates. Our investigation identified **Ru2** as a compound of particular interest. **Ru2** demonstrated remarkable cytotoxicity against MCF-7 breast cancer cells (IC_{50} = 0.28 μM), showing approximately 50-fold greater potency than cisplatin, while exhibiting improved selectivity for cancer over non-tumorigenic cells. The compound appears to act through mitochondrial disruption rather than DNA damage, as evidenced by $\Delta\psi_m$ collapse and the absence of nuclear morphological changes. This distinct mechanism was supported by negative results from the Ames and micronucleus assays, suggesting a potentially safer profile compared to traditional DNA-targeting agents. In more physiologically relevant 3D spheroid models, **Ru2** maintained dose-dependent activity, reducing tumor volume while maintaining selectivity. These results, although preliminary, warrant further investigation into the therapeutic potential of **Ru2**. While significant questions remain regarding *in vivo* efficacy and pharmacokinetics, **Ru2** represents an interesting addition to the growing field of non-platinum anticancer metallodrugs. Its combination of potency, selectivity and non-mutagenic properties makes it a candidate worthy of further investigation as we continue to develop improved cancer therapies.

Experimental

Materials and physical measurements

Reactions and chemicals were handled under an argon atmosphere. All chemicals used were of reagent grade or comparable purity. $RuCl_3{\cdot}3H_2O$, 1,1′-bis(diphenylphosphine)methane (dppm), 1,3-thiazolidine-2-thione (Hmtz), mercapto-1-methylimidazole (Hmmi) and 4,6-diamino-2-mercapto-pyrimidine (Hdmp) ligands were used as received from Sigma-Aldrich. The precursor *cis*-$[RuCl_2(dppm)_2]$ was prepared according to a published procedure.[30,31] The IR spectra were recorded using KBr pellets on a Bomem-Michelson 102 Fourier transform infrared spectrometer in the 4000–200 cm^{-1} region. Cyclic voltammetry experiments were performed using an EGeG Princeton Applied Research Model 273A electrochemical analyzer and were carried out at 25 °C. An electrochemical cell with a three-electrode system was used: a glassy carbon electrode as the working electrode, Ag/AgCl as the reference electrode, and a platinum plate as the auxiliary electrode. Tetrabutylammonium perchlorate (TBAP) at 0.10 M was used as a supporting electrolyte in DCM. Elemental analyses were performed at the Microanalytical Laboratory at the Universidade Federal de São Carlos, São Carlos, Brazil, using an EA 1108 CHNS microanalyzer (Fisons Instruments). Conductivity values were obtained, at 25 °C, using 1.0 mM solutions of the complexes in DCM with a Meter Lab CDM2300 instrument. $^{31}P\{^1H\}$, ^1H, $^{13}C\{^1H\}$, HSQC (^1H–^{13}C) and HMBC (^1H–^{13}C) NMR were recorded on a Bruker DRX 400 MHz spectrometer using DCM/D_2O or DMSO-d_6. The UV–Vis spectra of the complexes were recorded in DMSO on a Hewlett-Packard 8452A diode array. Mass spectrometry analyses were performed using an Agilent 6545 ESI-QTOF-MS instrument. The target MS/MS data were produced across the mass range of 50–1200 Da. Samples were dissolved in MeOH/0.1% formic acid and analyzed by FIA at a flow rate of 0.35 mL min^{-1} with a volume injection of 2.0 μL at 38 °C. The mobile phase consisted of H_2O + 0.1% formic acid and MeOH + 0.1% formic acid (20 : 80) with a 4.0 min analysis time.

Synthesis of the compounds

The complexes **Ru1–Ru3** were obtained from the *cis*-$[RuCl_2(dppm)_2]$ precursor.[26] In a Schlenk flask containing 20 mL of previously degassed methanol, 0.12 mmol of the respective mercapto ligand was added (Hmtz = 0.014 g; Hmmi = 0.014 g; Hdmp = 0.023 g) with 0.015 mmol of $NaHCO_3$ (0.018 g). Subsequently, 0.10 mmol (0.094 g) of the precursor *cis*-$[RuCl_2(dppm)_2]$ and 0.13 mmol (0.024 g) of KPF_6 were added to the flask. The system was kept under stirring and reflux for approximately 12 h. The volume of the solution was reduced to approximately 2 mL, and the yellow powder was filtered off, washed with water and ethyl ether, and dried under reduced pressure.

$[Ru(mtz)(dppm)_2]PF_6$ (Ru1). Yield: 113 mg, 94%. Elemental analysis (%) calc. for $C_{53}H_{48}F_6NP_5RuS_2$ [exp (calc)]: C, 56.18 (56.28); H, 4.27 (4.38); N, 1.24 (1.49); S, 5.66 (6.04). Molar conductance (μS cm^{-1}, DMSO): 55.9. IR (cm^{-1}): ν(C–H) 3054, $\nu(CH_2)$ 2856, ν(C=C + C=N) 1516–1432, ν(C–S) 1188, ν(P–C_{ring}) 1099, $\nu(PF_6^-)$ 836, 725, $\delta(PF_6^-)$ 559, ν(P–C) 522, ν(Ru–S) 480, ν(Ru–N) 423. ^{31}P $\{^1H\}$ NMR (162 MHz, DMSO-d_6): δ 3.79 (1P, ddd, J = 37.2, 33.7, 24.5 Hz), −1.13 (1P, ddd, J = 39.9, 32.5, 24.5 Hz), −17.29 (2P, ddd, J = 37.2, 32.5, 21.5 Hz), −144.70 (1P, hept, PF_6^-). UV–Vis [DMSO; λ(nm) $\varepsilon(M^{-1}\ cm^{-1})$]: 354 (2386; MLCT, d–d).

$[Ru(mmi)(dppm)_2]PF_6$ (Ru2). Yield: 105 mg, 87%. Elemental analysis (%) calc. for $C_{54}H_{49}F_6N_2P_5RuS$ [exp (calc)]: C, 57.50 (57.83); H, 4.38 (4.43); N, 2.48 (2.51); S, 2.84 (2.88). Molar conductance (μS cm^{-1}, DMSO): 57.7. IR (cm^{-1}): ν(C–H) 3054, $\nu(CH_2)$ 2868, ν(C=C + C=N) 1574–1435, ν(C–S) 1188, ν(P–

C_{ring}) 1096, $\nu(PF_6^-)$ 844, 728, $\delta(PF_6^-)$ 557, ν(P–C) 520, ν(Ru–S) 478, ν(Ru–N) 413. ^{31}P $\{^1H\}$ NMR (162 MHz, DMSO-d_6): δ 3.51–2.71 (1P, m), 1.81–1.03 (1P, m), −14.98 (1P, ddd, J = 319.8, 44.1, 25.0 Hz), −23.39 (1P, ddd, J = 319.8, 45.9, 28.4 Hz), −144.70 (1P, hept, PF_6^-). UV–Vis [DMSO; λ(nm) ε(M^{-1} cm^{-1})]: 346 (2849; MLCT), 408 (862; MLCT, d–d).

[Ru(dmp)(dppm)$_2$]PF$_6$ (Ru3). Yield: 97 mg, 79%. Elemental analysis (%) calc. for $C_{54}H_{49}F_6N_4P_5RuS$ [exp (calc)]: C, 56.11 (56.47); H, 4.27 (4.52); N, 4.85 (4.87); S, 2.77 (3.08). Molar conductance (μS cm^{-1}, DMSO): 60.0. IR (cm^{-1}): $\nu(NH_2)$ 3500, 3393, ν(C–H) 3152, 3053, $\nu(CH_2)$ 2986, ν(C=C + C=N) 1619–1433, ν(C–S) 1246, ν(P–C_{ring}) 1096, $\nu(PF_6^-)$ 844, 727, $\delta(PF_6^-)$ 560, ν(P–C) 518, ν(Ru–S) 480, ν(Ru–N) 416. ^{31}P $\{^1H\}$ NMR (162 MHz, DMSO-d_6): δ 0.16 (1P, ddd, J = 40.7, 28.4, 23.8 Hz), −12.26 to −12.97 (1P, m), −14.41 (1P, ddd, J = 327.8, 40.7, 24.5 Hz), −25.72 (1P, ddd, J = 327.8, 33.6, 28.4 Hz), −144.70 (1P, hept, PF_6^-). UV–Vis [DMSO; λ(nm) ε(M^{-1} cm^{-1})]: 318 (7853; MLCT), 364 (2944; MLCT), 412 (1302; MLCT, d–d).

X-Ray diffraction

The complexes were crystallized from methanol solutions by slow evaporation of the solvent. The measurements of single crystals were performed by X-ray diffraction using XTaLAB MINI (Rigaku) and APEX II (Bruker) diffractometers with graphite monochromated Mo Kα radiation (λ = 0.71073 Å). Cell refinements were carried out using the CrysalisPro[53] and Saint[54] software, and the structures were obtained by the intrinsic phasing method using the SHELXT[55] program. The Gaussian method was used for absorption corrections. Tables and structure representations were generated using OLEX2[56] and MERCURY,[34] respectively. The complexes exhibited positional disorder in the mercapto ligands for **Ru2** and in the PF_6^- counterion for all complexes, which were refined in two parts, totaling 100% occupancy. The **Ru1–Ru3** complexes exhibited positional disorder in the mercapto ligands and the PF_6^- counterion, which were refined in two parts, totaling 100% occupancy. CCDC codes: 2235452 (**Ru1**), 2235453 (**Ru2**) and 2235454 (**Ru3**).†

Stability in solution. The stability of **Ru1–Ru3** complexes was investigated using $^{31}P\{^1H\}$ NMR and UV-Vis spectroscopy. For the $^{31}P\{^1H\}$ NMR analyses, the complexes were studied in pure DMSO and in a DMSO/culture medium solution. Stock solutions of the complexes were diluted with Dulbecco's modified Eagle's medium (DMEM) to obtain final saturated solutions of the complexes with 90% DMSO (v/v). Regarding the UV-Vis measurements, the complexes were studied in DMEM without phenol red, in the presence of 10% fetal bovine serum (FBS). Stock solutions of the complexes were prepared in DMSO at 2000 μM and diluted with culture medium to obtain 100 μM and 5% DMSO (v/v) final solutions. Samples were analyzed immediately after preparation (0 h) and after 24 and 48 h.

Water/*n*-octanol distribution coefficient (log *P*). Water–octanol partition coefficients were determined using the shake-flask method.[57] A total of 1 mg of each complex was solubilized in 1000 μL of DMSO, and an aliquot of 50 μL was added to a mixture of equal volumes of water (975 μL) and *n*-octanol (975 μL). The solutions were continuously shaken for 24 h at 1000 rpm and 37 °C. Then, the samples were centrifuged for 5 min at 1000 rpm, and the organic and aqueous phases were separated. The organic phase was measured spectrophotometrically, and the concentration was determined from a calibration curve (linear regression) in order to obtain log *P* values = [complex(*n*-octanol)]/[complex(water)]. The experiments were carried out in triplicate.

Cell culture. The ruthenium complexes (**Ru1–Ru3**) were tested against human breast cancer cells MDA-MB-231 (ATCC HTB-26) and MCF-7 (ATCC HTB-22) and non-cancer breast cells MCF-10A (ATCC CRL-10317). The cells were routinely maintained in high-glucose DMEM (for MDA-MB-231), DMEM/F-12 (for MCF-10A) or Roswell Park Memorial Institute 1640 medium (RPMI 1640; for MCF-7), supplemented with 10% fetal bovine serum (FBS), at 37 °C under a humidified 5% CO_2 atmosphere. MCF-10A cells were maintained in DMEM/F-12 medium containing horse serum (HS) 5%, EGF (epidermal growth factor) (0.02 mg mL^{-1}), hydrocortisone (0.05 mg mL^{-1}) and insulin (0.01 mg mL^{-1}). The MDA-MB-231 cell line was purchased from the Rio de Janeiro Cell Bank (BCRJ). MCF-7 and MCF-10A cell lines were kindly provided by Marcia R. Cominetti, UFSCar, São Carlos, SP, Brazil. Cell culture media were obtained from Vitrocell, and FBS was obtained from Gibco.

***In vitro* cytotoxicity assay.** The cytotoxic activity of the complexes (**Ru1–Ru3**) was investigated *via* the 3-(4,5-dimethylthiazol-2-yl)-2,5-diphenyltetrazolium bromide (MTT) assay.[58] Cells were seeded in 150 μL of appropriate medium in 96-well plates and then incubated at 37 °C in 5% CO_2 for 24 h (1.5×10^4 cells per well). The complexes were dissolved in DMSO, and 0.75 μL was added to each well (final concentration of 0.5% DMSO per well). Cisplatin was prepared in an aqueous NaCl solution, and 0.75 μL was added to each well. The cells were incubated with the complexes for 48 h at 37 °C in 5% CO_2. Then, 50 μL of MTT (1 mg mL^{-1} in PBS) was added to each well, and the cells were incubated again for 4 h. After this period, the medium was removed, and formazan crystals were solubilized in isopropyl alcohol. Absorbance was measured using a BioTek Epoch microplate spectrophotometer at 540 nm. All compounds were tested in three independent experiments performed in triplicate. DMSO was used as the negative control. Cell viability was determined using GraphPad Prism 8.0.2 software.

Morphology assay. Cells (0.6×10^5 cells per well) were seeded in a 12-well plate and then incubated at 37 °C in 5% CO_2 for 24 h. After this period, the cells were treated with **Ru2** at IC_{50} and $2 \times IC_{50}$ concentrations (0.14 and 0.28 μM) and incubated for an additional 48 h. Cells were examined at 0 and 48 h under an inverted optical microscope (NIKON ECLIPSE TS100) with a 10× objective lens, coupled with a Motcam 1SP camera. The morphological changes of the cells exposed to the treatment were compared to those treated with the DMSO control.

Green Plasma/DAPI staining. Cells (1.0×10^4 cells per well) were seeded in a 96-well plate and then incubated at 37 °C in

5% CO_2 for 24 h. After this period, the cells were treated with **Ru2** at IC_{50} and 2 × IC_{50} concentrations (0.14 and 0.28 μM) and incubated for an additional 48 h. The cells were fixed with methanol and incubated with 80 μL (1 μg mL^{-1}) of Green Plasma (CellMask) and DAPI (4′,6-diamidino-2-phenylindole dilactate) for 1 h. Then, the images were taken using a CELENA® S Digital Imaging System (Logos Biosystems).

Live/dead assay. Cells (0.5×10^5 cells per well) were seeded in a 96-well plate and then incubated at 37 °C in 5% CO_2 for 24 h. After this period, the cells were treated with **Ru2** at IC_{50} and 2 × IC_{50} concentrations (0.14 and 0.28 μM) and incubated for an additional 48 h. Then, the cells were incubated with calcein-AM and propidium iodide (PI) for 1 h, and the images were taken using a CELENA® S Digital Imaging System (Logos Biosystems).

3D multicellular tumor spheroids (MCTSs). For the multicellular tumor spheroids (MCTSs) culture, the Greiner Bio-One's Magnetic 3D Cell Culture Bioprint Kit was used (Greiner Bio-One, Frickenhausen, Germany), which is based on the magnetization of cells with NanoShuttle-PL. In a 25 cm^2 culture flask containing MCF-7 cells, 80 μL of nanoparticle solution (NanoShuttle – PL) was added for magnetization. After 24 h, the cells were trypsinized, counted and seeded in a 96-well plate (1.5×10^3 cells per well). The plate was placed in a magnetic drive to obtain spheroids and incubated at 37 °C in 5% CO_2. The growth was observed using a CELENA® S Digital Imaging System (Logos Biosystems). After this period, **Ru2** was added at different concentrations (0.14, 0.28, 0.56, and 1.12 μM) and incubated for 6 days. The diameters of the spheroids were analyzed using ImageJ software and analyzed statistically using GraphPad Prism 8.0.2 software. For live/dead staining, the MCTSs were incubated with calcein-AM and propidium iodide (PI) for 1 h, and the images were taken using a CELENA® S Digital Imaging System (Logos Biosystems).

Clonogenic survival assay. Cells (0.4×10^3 cells per well) were seeded in a 6-well plate and then incubated at 37 °C in 5% CO_2 for 24 h. After this period, the cells were treated with **Ru2** at $\frac{1}{2}$ × IC_{50}, IC_{50} and 2 × IC_{50} concentrations (0.14–0.56 μM) and incubated for an additional 48 h. Then, the culture medium was replaced with fresh medium, and the plates were incubated for an additional 10 days. After this period, the culture medium was removed and the colonies formed were washed with PBS, fixed with a methanol/acetic acid (3 : 1) solution and then stained with violet crystal 0.5% in methanol for 30 min. Furthermore, the plates were washed with water and dried at 25 °C. The experiment was performed in triplicate. Relative survival was calculated using ImageJ software with the "*Colony Area*" plug-in and the "*Watershed*" and "*Analyze Particles*" functions. The parameters size (0.01–infinity) and circularity (0.30–1.00) were employed.

Transwell migration assay. Cells (0.5×10^5 cells per well) in serum-free medium were seeded on the upper chamber of Boyden transwell chambers containing **Ru2** at different concentrations ($\frac{1}{8}$ IC_{50}, $\frac{1}{4}$ IC_{50} and $\frac{1}{2}$ IC_{50}). Culture medium containing 10% FBS was added to the bottom chamber to act as a chemoattractant in the positive control of migration (C+). For the negative control of cell migration, serum-free medium was added to the lower chamber (C–). The transwell chambers were incubated at 37 °C in 5% CO_2 for 24 h. After that, the cells that migrated were fixed with methanol for 10 min, stained with DAPI and washed twice with distilled water. Images of the membrane were captured using the ImageXpress Micro microscope (Molecular Devices, San Jose, CA, USA) under 10× magnification with the meta-X-press software and quantified using the Multi-Wavelength Cell Scoring. The data show the mean number of cells that migrated in two independent experiments ± SD.

Gelatin zymography. To identify the gelatinolytic activity level of the metalloproteinases MMP-2 and MMP-9, cell culture supernatants (10 μg) were combined with non-denaturing sample buffer (glycerol 2%; EDTA 0.1 M; Tris 1M, bromophenol blue 0.03 mM, pH 6.8) in a 1 : 3 ratio. Aliquots of **Ru2** at $\frac{1}{8}$ IC_{50}, $\frac{1}{4}$ IC_{50} and $\frac{1}{2}$ IC_{50} concentrations were loaded onto a 10% SDS-PAGE gel containing gelatin (100 mg mL^{-1}) and subjected to a current of 85 V for approximately 3–4 hours at 4 °C. Using 2.5% Triton X-100, the gels were washed for 40 minutes at room temperature with constant agitation to remove excess SDS. Subsequently, the protein content present in the gels was renatured with incubation buffer (Tris 50 mM, $CaCl_2$ 5 mM, NaN_3 0.02%, $ZnCl_2$ 10 mM, pH 8.0) for 20 h at 37 °C, and the gels were stained with Coomassie Brilliant Blue (brilliant blue 0.25%, isopropanol 50%, acetic acid 10%) for 16 hours. The gels were washed in a destaining solution (acetic acid 10%, methanol 10%), and the proteolytic activity, characterized by the presence of colorless bands in the gels, was recorded using the ChemiDoc™ XRS+ (Bio-Rad) photodocumentor. Furthermore, quantification relative to the band density was performed using Image Lab software. Each sample was run on different gels ($n = 2$).

Cell cycle distribution. MCF-7 cells were plated (1.0×10^5 cells per well) in 12-well plates and incubated at 37 °C in 5% CO_2 for 24 h. The cells were treated with **Ru2** at $\frac{1}{2}$ × IC_{50}, IC_{50} and 2 × IC_{50} concentrations (0.14–0.56 μM) and incubated for an additional 48 h. Then, the cells were collected, washed twice with PBS and resuspended in ice-cold 70% ethanol (incubated at −20 °C for 24 h). Afterward, the cells were centrifuged, resuspended in a solution of RNase A (40 μg mL^{-1}) and PI (60 μg mL^{-1}) in PBS and incubated for 30 min. The DNA content was determined by flow cytometry using an ACCURI C5 cytometer (BD), with 10 000 events analyzed. Untreated cells served as the negative control.

Mitochondrial membrane potential. MCF-7 cells were seeded at a density of 1.0×10^4 cells per well in black 96-well plates (Corning) and maintained at 37 °C under a 5% CO_2 atmosphere for 24 h. The cells were treated with **Ru2** at IC_{50} and 2 × IC_{50} concentrations (0.14 and 0.28 μM) and incubated for an additional 24 h. After this period, the medium was removed and the cells were treated with a JC-1 solution (100 μL in RPMI 1640 medium without phenol red) and maintained at 37 °C under a 5% CO_2 atmosphere for 1 h. After incubation, the cells were washed with PBS, the fluorescence signal of JC-1 was read using a Synergy/H1-Biotek fluorometer (aggregate,

Ex/Em: 535/590 nm and monomer, Ex/Em: 475/530 nm), and the images were taken using a CELENA® S Digital Imaging System (Logos Biosystems). The data were analyzed using GraphPad Prism 8.0.2 software.

Apoptosis/necrosis assay. MCF-7 cells (1.5×10^5 cells per well) were seeded in 12-well plates (Corning) and incubated at 37 °C under a 5% CO_2 atmosphere for 24 h. The cells were treated with **Ru2** at $\frac{1}{2} \times IC_{50}$, IC_{50} and $2 \times IC_{50}$ concentrations (0.14–0.56 μM) and incubated for an additional 48 h. After this period, the cells were incubated with 2.5 μL of Annexin V-PE and 2.5 μL of 7-AAD (7-aminoactinomycin) for 15 minutes at room temperature in the dark. Analyses were performed using a BD Accurri C5 Plus flow cytometer, recording 15 000 events.

Genotoxicity studies

Ames test. The *Salmonella* mutagenicity assay (Ames test) was performed with *S. typhimurium* strains TA1535, TA98, TA100, TA102, and TA97a, with (+S9) and without (−S9) metabolic activation, using the preincubation method.[59] These strains were kindly provided by Dr B.N. Ames (Berkeley, CA, USA). For the experiments, the strains were grown overnight from frozen cultures for 16 h in Oxoid Nutrient Broth No. 2 (Thermo Fisher Scientific). The concentrations of **Ru2** (0.06 to 1.0 μM solubilized in DMSO) were selected based on preliminary toxicity tests with the TA100 strain. In all subsequent assays, the upper limit of the dose range tested was either the highest non-toxic dose or the lowest toxic dose determined in this preliminary assay. Toxicity was indicated either by a reduction in the number of His+ revertants or by an alteration in the auxotrophic background. The various concentrations of **Ru2** to be tested were added to 0.5 mL of 0.2 M phosphate buffer (pH 7.4) or 0.5 mL of 4% S9 mixture and 0.1 mL of bacterial culture and then incubated at 37 °C for 20–30 min. The metabolic activation mixture (S9 fraction), prepared from the livers of Sprague–Dawley rats treated with the polychlorinated biphenyl mixture Aroclor 1254 (500 mg kg^{-1}), was purchased from Molecular Toxicology Inc. (Boone, NC, USA) and freshly prepared before each test. The metabolic activation system consisted of 4% S9 fraction, 1% 0.4 M $MgCl_2$, 1% 1.65 M KCl, 0.5% 1 M D-glucose-6-phosphate disodium, 4% 0.1 M NADP, 50% 0.2 M phosphate buffer and 39.5% sterile distilled water. Thereafter, 2 mL of top agar was added, and the mixture was poured onto a plate containing minimal agar. The plates were incubated for 48 h at 37 °C, and the His+ revertant colonies were counted. The standard mutagens used as positive controls were 4-nitrophenylenediamine (24 μM) for the TA98 and TA97a strains, sodium azide (7 μM) for the TA1535 and TA100 strains and mitomycin C (0.53 μM) for the TA102 strain for experiments without the S9 mix and 2-anthramine (2.3 μM) for the TA1535, TA98, TA97a, and TA100 strains and 2-aminofluorene (20 μM) for the TA102 strain for the assays with metabolic activation. DMSO was used as the negative control (100 μL per plate). All experiments were performed in triplicate. The results were analyzed using the Salanal Statistical Program (US Environmental Protection Agency, Monitoring Systems Laboratory, Las Vegas, NV, version 1.0, from the Research Triangle Institute, RTP, North Carolina, USA). This program allows the evaluation of the dose–response effect by performing an analysis of variance (ANOVA) between the averages of the number of reversals at the different concentrations tested and the negative control, followed by linear regression.[60] The mutagenicity index (MI) also was calculated for each concentration tested, this being the mean number of revertants per plate with the test compound divided by the mean number of revertants per plate with the negative (solvent) control. The sample was considered mutagenic when a dose–response relationship was detected and a two-fold increase in the number of mutants ($MI \geq 2$) was observed for at least one concentration.[61]

Micronucleus assay. The human hepatocellular carcinoma HepG2 cell line used in the micronucleus assay was purchased from the American Type Cell Collection (ATCC® HB-8065™). The cells were cultured in low-glucose Dulbecco's modified Eagle's medium (DMEM). The culture medium was supplemented with 10% heat-inactivated fetal bovine serum (FBS) and 1% antibiotics. The cultured cells were maintained in a humidified incubator at 37 °C in 5% CO_2 and 96% of relative humidity. All the experiments were conducted between the third and the eighth cell passage. Cell detachment was performed by the addition of Trypsin–EDTA to the cultured cells. Before use in experiments, the viability of the cells was ascertained using the trypan blue exclusion technique with the Countess® Automated Cell Counter (Life Technologies, CA, USA). The mutagenic potential of the 1b complex was assessed as described by Fenech[62] with modifications, following the guidelines of the Organization for Economic Cooperation and Development (OECD).[63]

The HepG2 cells were seeded at a density of 5×10^5 per flask into 25 cm^2 culture flasks. Following the cell attachment to the flasks, the cells were rinsed and treated with three different concentrations (IC_{50} and two lower concentrations) of the **Ru2** complex. The positive control was treated with 0.05 μM doxorubicin (Sigma-Aldrich), while the negative control was treated with PBS in a culture medium. After 20 h of treatment (44 h after the initiation of the culture), the cells were washed with PBS, the culture medium was changed, and 4.0 μg mL^{-1} cytochalasin B (Sigma-Aldrich) was added to the cultures. The cells were then incubated for an additional 28 h, harvested with trypsin diluted in a cold hypotonic solution (0.01% sodium citrate), and fixed with formaldehyde and methanol–acetic acid (3 : 1 v/v) solution. The slides were stained immediately before analysis using a 40 μg mL^{-1} acridine orange (Sigma-Aldrich) solution. The cytokinesis-block proliferation index (CBPI) and the percentage cytotoxicity were calculated using the formulae:

$$\mathrm{CBPI} = [(\text{No. of mononucleate cells}) + (\text{No. of binucleate cells} \times 2) + (\text{No. of multinucleate cells} \times 3)]/\text{total No. of cells}$$

$$\%\text{Cytotoxicity} = 100 - 100[(\text{CBPI treatment} - 1)/(\text{CBPI negative control} - 1)]$$

The frequency of micronuclei (MNfreq) was calculated as the number of micronuclei per 1000 binucleated cells. Values

are shown as the mean ± SD and are based on three independent experiments.

Author contributions

Marcos V. Palmeira-Mello: conceptualization, investigation, methodology, validation, data curation, and writing – original draft. Tamara Teixeira: investigation. Analu R. Costa: investigation. Aline Maria Machado: investigation. Rone A. De Grandis: investigation. Leticia P. de Oliveira: investigation. Carlos André F. Moraes: investigation. João H. Araujo-Neto: investigation. Victor M. Deflon: Investigation. Adriano Defini Andricopulo: Methodology, formal analysis, and data curation. Javier Ellena: Methodology, formal analysis, and data curation. Heloisa S. Selistre-de-Araújo: Methodology, formal analysis, and data curation. Fillipe V. Rocha: funding acquisition, supervision and writing – review & editing. Alzir A. Batista: conceptualization, funding acquisition, supervision and writing – review & editing. All authors have approved the final version of the manuscript.

Data availability

The data supporting this article have been included as part of the ESI.†

Conflicts of interest

There are no conflicts to declare.

Acknowledgements

The authors are thankful for financial support from the following Brazilian Research Agencies: the São Paulo State Research Foundation (FAPESP, Grants 2023/02475-8 and 2022/02876-0) and the National Council for Scientific and Technological Development (CNPq). M. V. P.-M. thanks the São Paulo State Research Foundation (FAPESP, Grant 2021/01787-0). This study was partially funded by Coordenação de Aperfeiçoamento de Pessoal de Nível Superior – Brazil (CAPES) – Finance Code 001.

References

1 L. Kelland, The resurgence of platinum-based cancer chemotherapy, *Nat. Rev. Cancer*, 2007, **7**, 573–584.
2 S. Rottenberg, C. Disler and P. Perego, The rediscovery of platinum-based cancer therapy, *Nat. Rev. Cancer*, 2021, **21**, 37–50.
3 N. D. Eljack, H. M. Ma, J. Drucker, C. Shen, T. W. Hambley, E. J. New, T. Friedrich and R. J. Clarke, Mechanisms of cell uptake and toxicity of the anticancer drug cisplatin, *Metallomics*, 2014, **6**, 2126–2133.
4 R. Oun, Y. E. Moussa and N. J. Wheate, The side effects of platinum-based chemotherapy drugs: a review for chemists, *Dalton Trans.*, 2018, **15**, 6645–6653.
5 K. M. Kuznetsov, K. Cariou and G. Gasser, Two in one: merging photoactivated chemotherapy and photodynamic therapy to fight cancer, *Chem. Sci.*, 2024, **15**, 17760.
6 U. Das, U. Basu and P. Paira, Recent trends in the design and delivery strategies of ruthenium complexes for breast cancer therapy, *Dalton Trans.*, 2024, **53**, 15113.
7 Pragti, B. K. Kundu and S. Mukhopadhyay, Target based chemotherapeutic advancement of ruthenium complexes, *Coord. Chem. Rev.*, 2021, **448**, 214169.
8 S. Y. Lee, C. Y. Kim and T. G. Nam, Ruthenium Complexes as Anticancer Agents: A Brief History and Perspectives, *Drug Des., Dev. Ther.*, 2020, **3**, 5375–5392.
9 N. Nayeem, A. Yeasmin, S. N. Cobos, A. Younes, K. Hubbard and M. Contel, Investigation of the Effects and Mechanisms of Anticancer Action of a Ru(II)-Arene Iminophosphorane Compound in Triple Negative Breast Cancer Cells, *ChemMedChem*, 2021, **16**, 3280–3292.
10 S. Bonnet, Why develop photoactivated chemotherapy?, *Dalton Trans.*, 2018, **47**, 10330–10343.
11 J. Chen, Y. Zhang, X. Jie, J. She, G. Dongye, Y. Zhong, Y. Deng, J. Wang, B. Guo and L. Chen, Ruthenium(II) salicylate complexes inducing ROS-mediated apoptosis by targeting thioredoxin reductase, *J. Inorg. Biochem.*, 2019, **193**, 112–123.
12 R. Ye, Z. Ke, C. Tan, L. He, L. Ji and Z. Mao, Histone-deacetylase-targeted fluorescent ruthenium(II) polypyridyl complexes as potent anticancer agents, *Chem. – Eur. J.*, 2013, **19**, 31.
13 A. Notaro, M. Jakubaszek, N. Rotthowe, F. Maschietto, R. Vinck, P. S. Felder, B. Goud, M. Tharaud, I. Ciofini, F. Bedioui, R. F. Winter and G. Gasser, Increasing the Cytotoxicity of Ru(II) Polypyridyl Complexes by Tuning the Electronic Structure of Dioxo Ligands, *J. Am. Chem. Soc.*, 2020, **142**, 6066–6084.
14 J. Karges, F. Heinemann, M. Jakubaszek, F. Maschietto, C. Subecz, M. Dotou, R. Vinck, O. Blacque, M. Tharaud, B. Goud, E. V. Zahínos, B. Spingler, I. Ciofini and G. Gasser, Rationally Designed Long-Wavelength Absorbing Ru(II) Polypyridyl Complexes as Photosensitizers for Photodynamic Therapy, *J. Am. Chem. Soc.*, 2020, **142**, 6578–6587.
15 L. N. Lameijer, D. Ernst, S. L. Hopkins, M. S. Meijer, S. H. C. Askes, S. E. Le Dévédec and S. Bonnet, A Red-Light-Activated Ruthenium-Caged NAMPT Inhibitor Remains Phototoxic in Hypoxic Cancer Cells, *Angew. Chem., Int. Ed.*, 2017, **56**, 11549–11553.
16 U. Das, B. Kar, S. Pete and P. Paira, Ru(II), Ir(III), Re(I) and Rh(III) based complexes as next generation anticancer metallopharmaceuticals, *Dalton Trans.*, 2021, **50**, 11259.
17 P. Srivastava, M. Verma, A. Kumar, P. Srivastava, R. Mishra, S. Sivakumar and A. K. Patra, Luminescent naphthalimide-

tagged ruthenium(II)–arene complexes: cellular imaging, photocytotoxicity and transferrin binding, *Dalton Trans.*, 2021, **50**, 3629–3640.

18 D. Lovison, D. Alessi, L. Allegri, F. Baldan, M. Ballico, G. Damante, M. Galasso, D. Guardavaccaro, S. Ruggieri, A. Melchior, D. Veclani, C. Nardon and W. Baratta, Enantioselective Cytotoxicity of Chiral Diphosphine Ruthenium(II) Complexes Against Cancer Cells, *Chem. – Eur. J.*, 2022, **28**, e202200200.

19 M. Pernar, Z. Kokan, J. Kralj, Z. Glasovac, L. Tumir, I. Piantanida, D. Eljuga, I. Turel, A. Brozovic and S. I. Kirin, Organometallic ruthenium(II)-arene complexes with triphenylphosphine amino acid bioconjugates: Synthesis, characterization and biological properties, *Bioorg. Chem.*, 2019, **87**, 432–446.

20 A. Baysal, D. E. Karakas, N. Meric, B. Ak, M. Aydemir and F. Durap, Chiral phosphinites as efficient ligands for enantioselective Ru(II), Rh(I) and Ir(III)-catalyzed transfer hydrogenation reactions, *Transition Met. Chem.*, 2017, **42**, 365–372.

21 O. Tokgun, D. E. Karakas, S. Tan, E. R. Karagür, B. İnal, H. Akca, F. Durap, A. Baysal and M. Aydemir, Novel ruthenium and palladium complexes as potential anticancer molecules on SCLC and NSCLC cell lines, *Chem. Pap.*, 2020, **74**, 2883–2892.

22 R. J. Mitchell, A. S. Gowda, A. G. Olivelli, A. J. Huckaba, S. Parkin, J. M. Unrine, V. Oza, J. S. Blackburn, F. Ladipo, D. K. Heidary and E. C. Glazer, Triarylphosphine-Coordinated Bipyridyl Ru(II) Complexes Induce Mitochondrial Dysfunction, *Inorg. Chem.*, 2023, **62**, 10940–10954.

23 M. V. Palmeira-Mello, T. Teixeira, M. R. S. de Melo, H. D. Nicolella, J. L. Dutra, M. R. Cominetti, F. V. Rocha, D. C. Tavares and A. A. Batista, Ruthenium(II)-mercapto complexes induce cell damage via apoptosis pathway on ovarian cancer cells, *J. Inorg. Biochem.*, 2025, **265**, 112819.

24 M. M. da Silva, G. H. Ribeiro, M. S. de Camargo, A. G. Ferreira, L. Ribeiro, M. I. F. Barbosa, V. M. Deflon, S. Castelli, A. Desideri, R. S. Correa, A. B. Ribeiro, H. D. Nicolella, S. D. Ozelin, D. C. Tavares and A. A. Batista, Ruthenium(II) Diphosphine Complexes with Mercapto Ligands That Inhibit Topoisomerase IB and Suppress Tumor Growth In Vivo, *Inorg. Chem.*, 2021, **60**, 14174–14189.

25 K. M. Oliveira, E. J. Peterson, M. C. Carroccia, M. R. Cominetti, V. M. Deflon, N. P. Farrell, A. A. Batista and R. S. Correa, Ru(II)-Naphthoquinone complexes with high selectivity for triple-negative breast cancer, *Dalton Trans.*, 2020, **49**, 16193–16203.

26 V. D. S. Velozo-Sá, L. R. Pereira, A. P. D. Lima, F. Mello-Andrade, M. D. R. M. Rezende, R. M. Goveia, W. C. Pires, M. M. Silva, K. Oliveira, A. G. Ferreira, J. A. Ellena, V. M. Deflon, C. Grisolia, A. A. Batista and E. D. P. Silveira-Lacerda, *In vitro*, cytotoxicity and *in vivo* zebrafish toxicity evaluation of Ru(ii)/2-mercaptopyrimidine complexes, *Dalton Trans.*, 2019, **48**, 6026–6039.

27 M. M. Da Silva, M. S. De Camargo, R. S. Correa, S. Castelli, R. A. De Grandis, J. E. Takarada, E. A. Varanda, E. E. Castellano, V. M. Deflon, M. R. Cominetti, A. Desideri and A. A. Batista, Non-mutagenic Ru(ii) complexes: cytotoxicity, topoisomerase IB inhibition, DNA and HSA binding, *Dalton Trans.*, 2019, **48**, 14885–14897.

28 N. N. P. da Silva, M. V. Palmeira-Mello, N. O. Acesio, C. A. F. Moraes, J. Honorato, E. E. Castellano, D. C. Tavares, K. M. Oliveira and A. A. Batista, Ru(II)-diphosphine/N,S-mercapto complexes and their anti-melanoma properties, *Dalton Trans.*, 2025, **54**, 605–615.

29 G. H. Ribeiro, A. P. M. Guedes, T. D. de Oliveira, C. R. S. T. B. de Correia, L. Colina-Vegas, M. A. Lima, J. A. Nóbrega, M. R. Cominetti, F. V. Rocha, A. G. Ferreira, E. E. Castellano, F. R. Teixeira and A. A. Batista, Ruthenium (II) Phosphine/Mercapto Complexes: Their *in Vitro* Cytotoxicity Evaluation and Actions as Inhibitors of Topoisomerase and Proteasome Acting as Possible Triggers of Cell Death Induction, *Inorg. Chem.*, 2020, **59**, 15004–15018.

30 M. V. Palmeira-Mello, A. R. Costa, L. P. de Oliveira, O. Blacque, G. Gasser and A. A. Batista, Exploring the potential of ruthenium(II)–phosphine–mercapto complexes as new anticancer agents, *Dalton Trans.*, 2024, **53**, 10947.

31 M. V. Palmeira-Mello, P. Mesdom, P. Burckel, S. Hidalgo, O. Blacque, G. Gasser and A. A. Batista, Cytotoxic Ruthenium(II)-Diphosphine Complexes Affect the Mitochondrial Respiration of Lung Cancer Cells, *ChemBioChem*, 2025, **26**(2), e202400734.

32 K. Nakamoto, *Infrared and Raman Spectra of Inorganic and Coordination Compounds*, John Wiley, New York, 4rd edn, 1986.

33 W. J. Geary, *Coord. Chem. Rev.*, 1971, **7**, 81–122.

34 C. F. Macrae, I. Sovago, S. J. Cottrell, P. T. A. Galek, P. McCabe, E. Pidcock, M. Platings, G. P. Shields, J. S. Stevens, M. Towler and P. A. Wood, Mercury 4.0: from visualization to analysis, design and prediction, *J. Appl. Crystallogr.*, 2020, **53**, 226–235.

35 A. Saha, I. Mondal, A. Kumari, A. K. Sonkar, R. Mishra, R. Kulshreshtha and A. K. Patra, Hyphenation of lipophilic ruthenium(II)-diphosphine core with 5-fluorouracil: an effective metallodrug against glioblastoma brain cancer cells, *Dalton Trans.*, 2024, **53**, 1551–1567.

36 M. M. da Silva, M. S. de Camargo, S. Castelli, R. A. de Grandis, E. E. Castellano, V. M. Deflon, M. R. Cominetti, A. Desideri and A. A. Batista, Ruthenium(II)-mercapto Complexes with Anticancer Activity Interact with Topoisomerase IB, *J. Braz. Chem. Soc.*, 2020, **31**, 536–549.

37 R. Rouzier, C. M. Perou, W. F. Symmans, N. Ibrahim, M. Cristofanilli, K. Anderson, K. R. Hess, J. Stec, M. Ayers, P. Wagner, P. Morandi, C. Fan, I. Rabiul, J. S. Ross, G. N. Hortobagyi and L. Pusztai, Breast cancer molecular subtypes respond differently to preoperative chemotherapy, *Clin. Cancer Res.*, 2005, **11**, 5678–5685.

38 M. K. M. Subarkhan and R. Ramesh, Ruthenium(II) arene complexes containing benzhydrazone ligands: synthesis,

structure and antiproliferative activity, *Inorg. Chem. Front.*, 2016, **3**, 1245–1255.

39 T. Teixeira, M. V. Palmeira-Mello, P. H. Machado, C. A. F. Moraes, C. Pinto, R. C. Costa, W. Badaró, J. A. G. Neto, J. Ellena, F. Vieira Rocha, A. A. Batista and R. S. Correa, Ru(II)-Fenamic-Based Complexes as Promising Human Ovarian Antitumor Agents: DNA Interaction, Cellular Uptake, and Three-Dimensional Spheroid Models, *Inorg. Chem.*, 2025, **64**, 3707–3718.

40 H. Rafehi, C. Orlowski, G. T. Georgiadis, K. Ververis, A. El-Osta and T. C. Karagiannis, Clonogenic assay: adherent cells, *J. Visualized Exp.*, 2011, **13**(49), 2573.

41 J. Honorato, L. Colina-Vegas, R. S. Correa, A. P. M. Guedes, M. Miyata, F. R. Pavan, J. Ellena and A. A. Batista, Esterification of the free carboxylic group from the lutidinic acid ligand as a tool to improve the cytotoxicity of Ru(II) complexes, *Inorg. Chem. Front.*, 2019, **6**, 376–390.

42 C. Sonkar, S. Sarkar and S. Mukhopadhyay, Ruthenium(II)-arene complexes as anti-metastatic agents, and related techniques, *RSC Med. Chem.*, 2022, **13**, 22–38.

43 A. B. Becceneri, A. M. Fuzer, A. M. Plutin, A. A. Batista, S. A. Lelièvre and M. R. Cominetti, Three-dimensional cell culture models for metallodrug testing: induction of apoptosis and phenotypic reversion of breast cancer cells by the *trans*-[Ru(PPh_3)$_2$(*N*,*N*-dimethyl-*N*-thiophenylthioureato-k_2O,S)(bipy)]PF_6 complex, *Inorg. Chem. Front.*, 2020, **7**, 2909.

44 N. Gligorijević, S. Aranđelović, L. Filipović, K. Jakovljević, R. Janković, S. Grgurić-Šipka, I. Ivanović, S. Radulović and Ž. L. Tešić, Picolinate ruthenium(II)–arene complex with in vitro antiproliferative and antimetastatic properties: Comparison to a series of ruthenium(II)–arene complexes with similar structure, *J. Inorg. Biochem.*, 2013, **108**, 53–61.

45 Ş. Comșa, A. M. Cimpean and M. Raica, The Story of MCF-7 Breast Cancer Cell Line: 40 years of Experience in Research, *Anticancer Res.*, 2015, **35**(6), 3147–3154.

46 S. Sharkawy, A. Hernández-García, H. Kostrhunova, D. Bautista, L. Markova, M. D. Santana, J. Kasparkova, V. Brabec and J. Ruiz, A novel benzothiazole-1,2,3-triazole-based arene osmium(II) complex as an effective rhabdomyosarcoma cancer stem cell agent, *Inorg. Chem. Front.*, 2025, **12**, 1693.

47 J. Cervinka, A. Gobbo, L. Biancalana, L. Markova, V. Novohradsky, M. Guelfi, S. Zacchini, J. Kasparkova, V. Brabec and F. Marchetti, Ruthenium(II)–Tris-pyrazolylmethane Complexes Inhibit Cancer Cell Growth by Disrupting Mitochondrial Calcium Homeostasis, *J. Med. Chem.*, 2022, **65**(15), 10567–10587.

48 Food & Drug Administration, *Redbook 2000: IV.C.9.a. Bacterial Reverse Mutation Test. Toxicological Principles for the Safety Assessment of Food Ingredients*, 2018, vol. 23, pp. 1–18.

49 OECD 471. Bacterial Reverse Mutation Test. OECD Guideline for testing of chemicals, July, 1997.

50 M. Kwon, M. L. Leibowitz and J. H. Lee, Small but mighty: the causes and consequences of micronucleus rupture, *Exp. Mol. Med.*, 2020, **52**, 1777–1786.

51 J. W. Lee, H. J. Lee, Y. Lee, Y. Lim, W. J. Sim, J. Jang, H. Heo, H. Lim, J. Jung and J. S. Kim, Determination of Genotoxicity Attributed to Diesel Exhaust Particles in Normal Human Embryonic Lung Cell (WI-38) Line, *Biomolecules*, 2021, **11**, 291.

52 R. A. de Grandis, A. R. Costa, C. A. F. Moraes, N. Z. Sampaio, I. H. Cerqueira, W. G. Marques, A. P. M. Guedes, J. Araujo-Neto, F. R. Pavan, F. C. Demidoff, C. D. Netto, A. A. Batista and F. A. Resende, Novel Ru(II)-bipyridine/phenanthroline-lapachol complexes as potential anti-cancer agents, *J. Inorg. Biochem.*, 2022, **237**, 112005.

53 Agilent, *CrysAlis PRO*, Agilent Technologies Ltd, Yarnton, Oxfordshire, England, 2014.

54 Bruker, *SAINT*, Bruker AXS Inc., Madison, Wisconsin, USA, 2012.

55 G. M. Sheldrick, SHELXT - integrated space-group and crystal-structure determination, *Acta Crystallogr., Sect. A: Found. Adv.*, 2015, **71**, 3–8.

56 O. V. Dolomanov, L. J. Bourhis, R. J. Gildea, J. A. K. Howard and H. Puschmann, OLEX2: a complete structure solution, refinement and analysis program, *J. Appl. Crystallogr.*, 2009, **42**, 339–341.

57 E. Baka, J. E. A. Comer and K. Takács-Novák, Study of equilibrium solubility measurement by saturation shake-flask method using hydrochlorothiazide as model compound, *J. Pharm. Biomed. Anal.*, 2008, **46**, 335–341.

58 T. Mosmann, Rapid colorimetric assay for cellular growth and survival: application to proliferation and cytotoxicity assays, *J. Immunol. Methods*, 1983, **65**, 55–63.

59 D. M. Maron and B. N. Ames, Revised methods for the Salmonella mutagenicity test, *Mutat. Res.*, 1983, **113**, 173–215.

60 L. Bernstein, J. Kaldor, J. McCann and M. C. Pike, An empirical approach to the statistical analysis of mutagenesis data from the Salmonella test, *Mutat. Res.*, 1982, **97**, 267–281.

61 K. Mortelmans and E. Zeiger, The Ames Salmonella/microsome mutagenicity assay, *Mutat. Res.*, 2000, **455**, 29–60.

62 M. Fenech, Cytokinesis-block micronucleus cytome assay, *Nat. Protoc.*, 2007, **2**, 1084–1104.

63 OECD 487. In Vitro Mammalian Cell Micronucleus Test. OECD Guideline for the Testing of Chemicals, July, 2016.

